AIAA AVIATION Forum
5-9 June 2017, Denver, Colorado
23rd AIAA Computational Fluid Dynamics Conference

10.2514/6.2017-3447

Check for updates

An Embedded Robin Boundary Method for Incompressible Fluid-Structure Interaction Problems

Shunxiang Cao,* Alex Main, † Kevin Wang ‡
*‡ *Virginia Polytechnic Institute and State University, Blacksburg, VA, 24060, USA*
† *Duke University, Durham, NC, 27708, USA*

Partitioned procedures are widely used in the solution of fluid-structure interaction (FSI) problems, primarily because they facilitate the use of advanced numerical algorithms and computational codes developed specifically for each sub-system. However, numerical instability is a major issue, especially when the fluid is incompressible, and the fluid-structure density ratio is large. In this paper, we present a numerically stable partitioned procedure featuring a Robin-Neumann interface condition and an embedded boundary method. First introduced in Badia *et al.*,[1] the one-parameter Robin-Neumann interface condition has been shown to significantly mitigate the numerical added-mass effect when the model parameter introduced to the Robin boundary condition is carefully selected. In this work, we apply this approach to an embedded boundary method for FSI problems with complex geometry, large structural deformation, and/or topological change (e.g., fracture). Specifically, we first consider a two-dimensional FSI model for which the exact solution can be derived in closed-form formulation. Using this model, we mathematically analyze the effect of the aforementioned model parameter on numerical stability, and derive its optimal value. Next, we present the numerical algorithms to enforce the Robin-Neumann interface condition for general incompressible FSI problems, in the context of embedded boundary method. The salient features of the proposed numerical method will also be assessed using the Turek-Hron benchmark problem.

Nomenclature

α	non-dimensional combination parameter
α_f	combination parameter of Robin transmission condition
$\bar{\mathbf{K}}$	state vector of beam kinematics
Δt	time step size, s
η	density ratio
$\Gamma_L, \Gamma_R, \Gamma_B$	left, right, bottom boundary of fluid domain
λ	eigenvalue
ω	frequency of beam, rad/s
ω_0	natural frequency of beam, rad/s
Ω_s, Ω_f	structure domain, fluid domain
Φ	numerical stability quantity
ρ_s, ρ_f	structure density, fluid density, kg/m^3
Σ	fluid-structure interface
$\tilde{w}$	vibration magnitude of beam, m
$\mathbf{n}$	unit normal
$\mathbf{U}$	fluid velocity, m/s

*Graduate Student, Department of Aerospace and Ocean Engineering, Randolph Hall, Room 332, Virginia Tech, Blacksburg, VA 24060, USA
†Post-Doctoral Scholar, Department of Civil and Environmental Engineering, Duke University, Durham, NC 27708, USA
‡Assistant Professor, Department of Aerospace and Ocean Engineering, Randolph Hall, Room 332-3, Virginia Tech, Blacksburg, VA 24060, USA

Copyright © 2017 by the American Institute of Aeronautics and Astronautics, Inc. All rights reserved.

Downloaded by VIRGINIA TECH on July 12, 2018 | http://arc.aiaa.org | DOI: 10.2514/6.2017-3447

a vertical acceleration of beam, m/s^2
b, h width, height of beam, m
C_h, C_H non-dimensional parameter
E Young's modulus, kg/(ms^2)
f flow-induce force, N
I second moment of area of beam cross-section, m^4
k wave number
L, H length, height of fluid domain, m
P fluid pressure, Pa
t time, s
v vertical velocity of beam, m/s
W, w beam vertical displacement, m
x, y Cartesian coordinates

Subscripts

c critical value
n time step index
opt optimal value

Downloaded by VIRGINIA TECH on July 12, 2018 | http://arc.aiaa.org | DOI: 10.2514/6.2017-3447

I. Introduction

Nonlinear fluid-structure interaction (FSI) is an important phenomenon underlying many aerospace and oceanic vehicle designs such as those utilizing flexible, reconfigurable, and morphing structures. In order to achieve high performance at low cost, this phenomenon needs to be rigorously analyzed, and properly accounted for early in the design process. Numerical methods for solving coupled fluid-solid problems fall into two categories: those that employ a monolithic procedure, and those employing a partitioned one.[2–7] In the monolithic procedure,[2,3] the fluid and structure governing equations are semi-discretized and time-integrated simultaneously as one system. This approach can account for the strong coupling between the two subsystems, but requires a fully-integrated fluid-structure solver. On the other hand, the partitioned procedure[4–7] solves the fluid and structure governing equations separately. Specifically, a CFD (computational fluid dynamics) solver and a CSD (computational structural dynamics) solver can be used for the separate evaluations of the two subsystems, while the kinematic and dynamic interface conditions, also referred to as transmission conditions, are enforced through data exchange between the two solvers.

Within the category of partitioned procedures, *explicit coupling schemes* (also referred to as "loose" coupling) solve the fluid and the structure governing equations once per time step, without sub-iteration. Figure 1 illustrates the solution and data exchange of this type of schemes using asynchronous time grids. Specifically, at the fluid-structure interface, the velocity of the fluid is prescribed to be the velocity of the structure computed by the CSD solver, while the traction on the surface of the structure is computed using the fluid pressure and viscous stress. In other words, the kinematic and dynamic interface conditions are enforced by applying a Dirichlet boundary condition in the fluid subsystem and a Neumann boundary condition in the structure subsystem. This type of Dirichlet-Neumann (D-N) explicit coupling scheme has been successfully used in modeling and simulating many compressible fluid-structure interaction problems.[8–13] However, for FSI problems involving incompressible flows and light structures, a particular numerical instability (often referred to as the artificial or numerical added-mass effect) is a major issue, which has been formulated and studied in Causin *et al.*[6] and Főrster *et al.*[7] It has been discovered that when the densities of the fluid and structure are comparable (or that the solid is less dense than the fluid) the loose coupling approach results in an unconditionally unstable scheme. A straightforward method to fix this issue is to perform multiple (often > 10) subiterations between the fluid and structure solvers in the fashion of fixed-point iteration. This approach is often referred to as implicit or "strong" coupling. However, the resulting high computation cost limits the scope of applications.[6]

To mitigate the numerical added-mass effect without significantly increasing the computational cost, several ideas have been proposed in the past few years. An explicit coupling scheme, referred to as the kinematically coupled scheme, was proposed in Guidoboni *et al.*[15] and then extended to kinematically coupled β - scheme in Bukač *et al.*[16] with improved accuracy. This type of methods enforce the kinematic interface condition implicitly in a Lie's time-splitting scheme. The resulting fluid subsystem includes structure inertia, which is thought to be the main reason for the improved stability of the scheme.[17] However, this approach

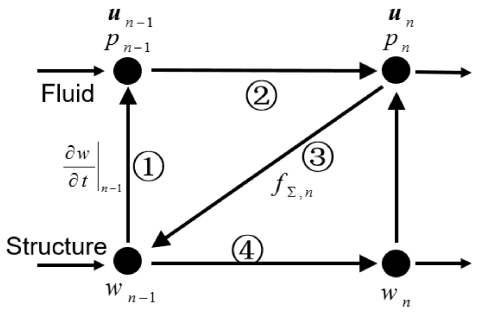

Figure 1: Dirichlet-Neumann explicit coupling scheme.[14]

has poor software modularity in the sense that the decoupled systems are no longer a pure fluid subsystem and a pure structure subsystem. A semi-implicit coupling scheme was introduced in Fernández *et al.*[18] to reduce the number of fluid-structure iterations in the implicit coupling scheme without compromising the numerical stability. The idea is to apply an implicit coupling scheme to the main source of the added-mass effect: the strong coupling of fluid pressure and the structural velocity - while the fluid convection, diffusion and domain motion are treated explicitly by applying the simple explicit coupling scheme. However, doing this still requires solving parts of the fluid subsystem with structure subsystem monolithically.
Badia *et al.*[1] proposed a novel approach in which the Dirichlet transmission condition for the fluid solver is replaced by a Robin transmission condition, that is, a linear combination of the kinematic and dynamic interface conditions. In comparison with the other two methods reviewed above, this Robin-Neumann scheme exhibits remarkable stability properties under strong added-mass effect so long as the linear combination parameter is carefully selected. Furthermore, since it only requires modifying the boundary condition of the fluid subsystem, the Robin-Neumann scheme is beneficial from a software development standpoint.

The Robin-Neumann scheme has been applied in Arbitrary Lagrangian Eulerian (ALE) frameworks[1,19,20] and in the context of overlapping grids.[21] In this work, we apply this scheme to an embedded boundary method, which is particularly suitable for FSI problems involving complex geometry, large structural deformation, and topological change (e.g., fracture).[8–13] In addition, we quantify the effect of the choice of the linear combination parameter on the accuracy and stability of the scheme. While previous work has shown that the stability of the Robin-Neumann scheme is sensitive to the linear combination parameter in the Robin boundary condition, in this work we will characterize the effects of this parameter by means of analyzing a simplified two-dimensional (2D) FSI model problem which can be solved analytically.

The remainder of this paper is organized as follows. Section II presents a mathematical analysis of the Robin boundary condition, independent of specific spatial discretization schemes (e.g., finite element, finite difference, etc.) and time integrators (explicit, implicit), using a 2D model problem involving incompressible, inviscid flow and an Euler-Bernoulli beam. Section III presents the proposed Embedded Robin Boundary Method (ERBM) for the interaction of incompressible viscous flows and deformable structures and the simulation result of . To verify and validate the proposed numerical methods, simulation result of the well-known Turek-Hron benchmark problem is also presented.

II. A 2-Dimensional Fluid-structure Interaction Model

A. Model Problem

As a model problem, we consider the interaction of a flexible linear beam with an inviscid, incompressible flow, for which exact solution can be derived in closed form. The objective is twofold. First, we aim to analyze the stability property of the Robin-Neumann scheme, including the effect of the linear combination parameter in the Robin boundary condition, independently of specific spatial discretization schemes and time integrators. Second, we aim to derive in closed form the optimal value of the aforementioned model parameter, and use this formula to set the parameter value for general incompressible FSI problems.

Let Ω_s be the structure domain, occupied by a simply-supported Euler-Bernoulli beam. The fluid occupies a 2D rectangular domain $\Omega_f = (0, L) \times (0, H)$ with length L and height H. Ω_f has a common boundary with Ω_s at its top boundary, which is the fluid-structure interface denoted by $\Sigma = \partial\Omega_f \cap \partial\Omega_s$ (see figure 2). We

Downloaded by VIRGINIA TECH on July 12, 2018 | http://arc.aiaa.org | DOI: 10.2514/6.2017-3447

assume that the left and right boundaries of Ω_f are periodic. Moreover, because the structural deformation is small, we neglect the variation of Ω_f in time. For simplicity, we only consider transverse displacements of the beam. With these assumptions, the model problem reads:
Find $W = W(x,t)$, $\mathbf{U} = \mathbf{U}(x,y,t)$, $P = P(x,y,t)$ such that

$$\begin{cases} EI\dfrac{\partial^4 W}{\partial x^4} + \rho_s bh\dfrac{\partial^2 W}{\partial t^2} = f & \text{in } (0,T)\times\Omega_s \quad (1a)\\ \rho_f\dfrac{\partial \mathbf{U}}{\partial t} + \nabla P = 0 & \text{in } (0,T)\times\Omega_f \quad (1b)\\ \nabla\cdot\mathbf{U} = 0 & \text{in } (0,T)\times\Omega_f \quad (1c)\\ \mathbf{U}\cdot\mathbf{n} = 0 & \text{on } \Gamma_B \quad (1d)\\ \dfrac{\partial P}{\partial n}|_{\Gamma_L} = \dfrac{\partial P}{\partial n}|_{\Gamma_R},\ P|_{\Gamma_L} = P|_{\Gamma_R} & \quad (1e)\end{cases}$$

where ρ_f is fluid density, W denotes transverse displacements of the beam, $\mathbf{U}$ fluid velocity and P fluid pressure; Γ_L, Γ_R, Γ_B denote the left, right and bottom boundary of Ω_f, respectively. E denotes the Young's modulus of the beam material and I the second moment of the area of the beams cross-section. ρ_s is the beam density, h and b denote the height and width of the beam, respectively. f is the flow-induced force on the beam. The beam is pinned on both ends, which gives $W|_{\partial\Omega_s} = \partial^2 W/\partial x^2|_{\partial\Omega_s} = 0$. On the interface Σ, the kinematic and dynamic interface conditions are given by Eq.(1f) and Eq.(1g), respectively.

$$\begin{cases} \mathbf{U}\cdot\mathbf{n} = \dfrac{\partial W}{\partial t}(x,t) & \text{on } \Sigma \quad (1f)\\ f = P|_\Sigma b & \text{on } \Sigma \quad (1g)\end{cases}$$

where the vector $\mathbf{n}$ is the outward unit normal from the fluid domain. Since we only consider vertical displacement of beam, $\mathbf{n} = (0,1)$.

Since fluid velocity is solenoidal, it can be eliminated from the coupled system Eq.(1) , resulting in the pressure Poisson equation. The reformulated system is written as Eq.(2).

$$\begin{cases} EI\dfrac{\partial^4 W}{\partial x^4} + \rho_s bh\dfrac{\partial^2 W}{\partial t^2} = f & \text{in } (0,T)\times\Omega_s \quad (2a)\\ W|_{\partial\Omega_s} = \dfrac{\partial^2 W}{\partial x^2}|_{\partial\Omega_s} = 0 & \quad (2b)\\ \nabla^2 P = 0 & \text{in } (0,T)\times\Omega_f \quad (2c)\\ \dfrac{\partial P}{\partial y} = 0 & \text{on } \Gamma_B \quad (2d)\\ \dfrac{\partial P}{\partial y}|_{\Gamma_L} = \dfrac{\partial P}{\partial y}|_{\Gamma_R},\ P|_{\Gamma_L} = P|_{\Gamma_R} & \quad (2e)\\ \dfrac{\partial P}{\partial y} = -\rho_f\dfrac{\partial^2 W}{\partial t^2} & \text{on } \Sigma \quad (2f)\\ f = P|_\Sigma b & \text{on } \Sigma \quad (2g)\end{cases}$$

A closed-form formulation of the exact solution can be derived and we refer the reader to Banks *et al.*[22]

B. Partitioned Solution and Mathematical Analysis

In this section, we solve the 2D model problem using two explicit partitioned procedures based on different transmission conditions, i.e., Dirichlet-Neumann (D-N) explicit coupling scheme and Robin-Neumann (R-N) explicit coupling scheme. Note that, in the following paper, "partitioned solution" is used to refer to numerical solution based on partitioned procedure. Furthermore, mathematical analysis is carried out to study the differences in stability properties and accuracy between these two partitioned procedures. Most importantly, we characterize the effect of combination parameter on stability and accuracy in R-N explicit coupling scheme and propose a method to determine its optimal value.

Downloaded by VIRGINIA TECH on July 12, 2018 | http://arc.aiaa.org | DOI: 10.2514/6.2017-3447

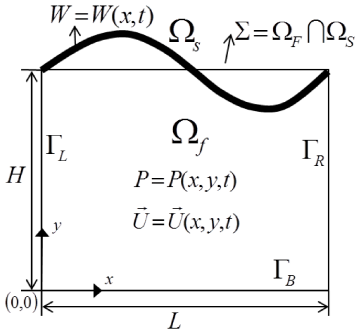

Figure 2: Geometry of FSI model problem

1. Dirichlet-Neumann (D-N) explicit coupling scheme

We first consider the D-N explicit coupling scheme in which the coupled system Eq.(2) is separated into a fluid subsystem with a Dirichlet transmission condition and the structure subsystem with a Neumann transmission condition. At each time step, we consider using an explicit asynchronous manner for the separate evaluations of fluid and structure subsystems (see figure 1). One novelty in this work is that, at each time step, instead of solving fluid and structure equations using a specific spatial discretization scheme or time integrator, we solve them analytically. This allows the partitioned procedure to be assessed independently of any spatial discretizations or time integrators. Before describing the algorithm, we first define following notation:

(1) Partitioned solution (functions in time) at time step $t \in [t_{n-1}, t_n]$:

Fluid pressure: $P_n = P_n(x, y, t)$;

Beam displacement: $W_n = W_n(x, t)$;

(2) Partitioned solution at time t_n;

Fluid pressure on Σ: $p_n = P_n(x, H, t_n)$;

Beam displacement: $w_n = W_n(x, t_n)$;

Beam velocity: $v_n = \dfrac{\partial w_n}{\partial t} = \dfrac{\partial W_n}{\partial t}|_{t_n}$;

Beam acceleration: $a_n = \dfrac{\partial^2 w_n}{\partial t^2} = \dfrac{\partial^2 W_n}{\partial t^2}|_{t_n}$;

Algorithm 1: Assuming initial conditions at t_{n-1} to be given as Eq.(3) , the algorithm at time step $t \in [t_{n-1}, t_n]$ reads as follows:

$$W_n(x, t_{n-1}) = w_{n-1}, \qquad \frac{\partial W_n}{\partial t}|_{t_{n-1}} = \frac{\partial w_{n-1}}{\partial t}, \qquad \frac{\partial^2 W_n}{\partial t^2}|_{t_{n-1}} = \frac{\partial^2 w_{n-1}}{\partial t^2} \tag{3}$$

Step 1: Transfer structure kinematics at t_{n-1} to fluid subsystem as the boundary condition;

$$\frac{\partial P_n}{\partial y} = -\rho_f \frac{\partial^2 w_{n-1}}{\partial t^2} \qquad on\, \Sigma \tag{4}$$

Step 2: Advance the fluid subsystem to t_n by solving fluid equations Eq.(4) and Eq.(5) analytically;

$$\begin{cases} \nabla^2 P_n = 0 & \text{in}\, \Omega_f \quad (5a) \\ \dfrac{\partial P_n}{\partial y} = 0 & \text{on}\, \Gamma_B \quad (5b) \\ P_n|_{\Gamma_L} = P_n|_{\Gamma_R} \quad (5c) \\ \dfrac{\partial P_n}{\partial y}|_{\Gamma_L} = \dfrac{\partial P_n}{\partial y}|_{\Gamma_R} \quad (5d) \end{cases}$$

Downloaded by VIRGINIA TECH on July 12, 2018 | http://arc.aiaa.org | DOI: 10.2514/6.2017-3447

Step 3: Compute the flow-induced pressure on interface Σ and transfer it to structure;

$$f_n = p_n b \qquad \text{on } \Sigma \tag{6}$$

Step 4: Advance the structure subsystem to t_n by solving structure equations Eq.(6) and Eq.(7) analytically.

$$\begin{cases} EI\dfrac{\partial^4 W_n}{\partial x^4} + \rho_s bh\dfrac{\partial^2 W_n}{\partial t^2} = f_n \qquad \text{in } \Omega_s & \text{(7a)} \\ W_n|_{\partial\Omega_s} = \dfrac{\partial^2 W_n}{\partial x^2}|_{\partial\Omega_s} = 0 & \text{(7b)} \end{cases}$$

We now analyze the stability properties by referring to the work of Banks *et al.*[22] First, referring to the problem setup, the partitioned solution at each time step can be expanded into a Fourier sine series:

$$W_n(x,t) = \sum_{i=1}^{\infty} \hat{W}_n(k,t)\sin(kx), \qquad P_n(x,y,t) = \sum_{i=1}^{\infty} \hat{P}_n(k,y,t)\sin(kx) \tag{8}$$

where $k = 2\pi i/L$ and hat functions represent the amplitude of corresponding sine wave. For one Fourier component that corresponds to one wavenumber k, the structure governing equation Eq.(7a) can be reformulated by:

$$EIk^4\hat{W}_{n,k}(t) + \rho_s bh\frac{\partial^2 \hat{W}_{n,k}(t)}{\partial t^2} = \hat{P}_{n,k}(H,t_n)b = \hat{p}_{n,k}b \tag{9}$$

In the following, we only consider one Fourier component and ignore the subscript k. With the new pressure on interface Σ computed in Step 3, solving Eq.(9) corresponds to solving the following second-order linear ordinary differential equation (ODE):

$$\frac{\partial^2 \hat{W}_n(t)}{\partial t^2} + \omega_0^2\hat{W}_n(t) = \frac{M_a}{\rho_s h}\frac{\partial^2 \hat{w}_{n-1}}{\partial t^2} \tag{10}$$

where $\omega_0 = \sqrt{EIk^4/(\rho_s bh)}$, $M_a = -\rho_f/[k\tanh(kH)]$. Let's denote the initial state of beam at t_{n-1} by $\hat{\mathbf{K}}_{n-1} = (\hat{w}_{n-1}, \hat{v}_{n-1}, \hat{a}_{n-1})^T$. The final state $\hat{\mathbf{K}}_n = (\hat{w}_n, \hat{v}_n, \hat{a}_n)^T$ can be obtained by solving the ODE Eq.(10) analytically, which can be expressed as a linear system of beam kinematics Eq.(11).

$$\begin{bmatrix} \hat{w}_n \\ \hat{v}_n \\ \hat{a}_n \end{bmatrix} = \mathbf{C_{DN}} \begin{bmatrix} \hat{w}_{n-1} \\ \hat{v}_{n-1} \\ \hat{a}_{n-1} \end{bmatrix} = \begin{bmatrix} \cos(\omega_0\Delta t) & \frac{\sin(\omega_0\Delta t)}{\omega_0} & \frac{M_a b[1-\cos(\omega_0\Delta t)]}{EIk^4} \\ -\omega_0\sin(\omega_0\Delta t) & \cos(\omega_0\Delta t) & \frac{M_a\omega_0 b\sin(\omega_0\Delta t)}{EIk^4} \\ -\omega_0^2\cos(\omega_0\Delta t) & -\omega_0\sin(\omega_0\Delta t) & \frac{M_a\omega_0^2 b\cos(\omega_0\Delta t)}{EIk^4} \end{bmatrix} \begin{bmatrix} \hat{w}_{n-1} \\ \hat{v}_{n-1} \\ \hat{a}_{n-1} \end{bmatrix} \tag{11}$$

Hence, given an initial condition at t_0, the partitioned solution at certain t_n can be computed explicitly using Eq.(11).

The stability properties of the above linear system Eq.(11) are determined by spectral radius of matrix $\mathbf{C_{DN}}$. The error is bounded if all of the eigenvalues λ of the matrix $\mathbf{C_{DN}}$ satisfy $|\lambda| \leq 1$. Hence, the stability criterion of D-N explicit coupling scheme is given by Eq.(12).

$$|\rho(\mathbf{C_{DN}})| \approx \Phi_{DN} = \frac{\cosh(kH)}{\eta hk\sinh(kH)} \leq 1 \tag{12}$$

where $\eta = \rho_s/\rho_f$. Moreover, $|\rho(\mathbf{C_{DN}})| = \Phi_{DN}$ if Δt goes to zero. It can be seen from Eq.(12) that the numerical stability of D-N explicit coupling scheme depends on the density ratio η between structure and fluid, the thickness of beam h, the height of fluid domain H and the wavenumber k. The scheme becomes unstable if the added-mass effect is significant, e.g., involving a small density ratio and/or a slender domain. This result is similar to those results in Causin *et al.*,[6] Főrster[7] *et al.*, Banks *et al.*[22] but it is independent of the spatial discretization scheme and time integrator for each subsystem.

Downloaded by VIRGINIA TECH on July 12, 2018 | http://arc.aiaa.org | DOI: 10.2514/6.2017-3447

Downloaded by VIRGINIA TECH on July 12, 2018 | http://arc.aiaa.org | DOI: 10.2514/6.2017-3447

2. Robin-Neumann (R-N) explicit coupling scheme

As we have already seen, numerical instability is encountered in the D-N explicit coupling scheme for problems with a significant added-mass effect. An alternative is to use the R-N explicit coupling scheme based on Robin transmission condition, which is a linear combination of the kinematic and dynamic conditions at fluid-structure interface. First proposed in Badia et al.,[1] R-N schemes have shown remarkable stability properties when the added-mass effect is a potential pitfall as long as the linear combination parameter is carefully selected. The R-N scheme splits the coupled system into a fluid subsystem with Robin transmission condition and a structure subsystem with Neumann transmission condition. We now consider using the R-N explicit coupling scheme to solve the coupled system Eq.(2). The new algorithm is the same as **Algorithm 1** except that the boundary condition of the fluid subsystem Eq.(4) is replaced by a Robin transmission condition, i.e., a linear combination of kinematic Eq.(2f) and dynamics conditions Eq.(2g).

$$\alpha_f \frac{\partial P_n}{\partial y} + P_n b = p_{n-1} b - \alpha_f \rho_f \frac{\partial^2 w_{n-1}}{\partial t^2} \qquad \text{on } \Sigma \tag{13}$$

where α_f is the linear combination parameter that satisfies $\alpha_f > 0$. By taking $\alpha_f = \infty$, R-N explicit coupling scheme coincides with D-N explicit coupling scheme. It has been shown that stability properties of R-N schemes depend on the choice of α_f.[1] Thanks to the simple nature of 2D model problem, we now provide a mathematical analysis on the effect of combination parameter α_f on the numerical stability properties and the accuracy of Robin-Neumann explicit coupling scheme.

First, we apply the same strategy (Eq.(8)-Eq.(12)) to analyze the effect on stability properties. With the new Robin transmission condition, the second-order linear ODE corresponds to Eq.(10) is given by Eq.(14).

$$\frac{\partial^2 \hat{W}_n(t)}{\partial t^2} + \omega_0^2 \hat{W}_n(t) = M_1 \omega_0^2 \hat{w}_{n-1} + M_2 \omega_0^2 \frac{\partial^2 \hat{w}_{n-1}}{\partial t^2} \tag{14}$$

where M_1 and M_2 are defined as:

$$M_1 = \frac{1}{\alpha_f k \tanh(kH)/b + 1}, \qquad M_2 = \frac{\rho_s bh - \alpha_f \rho_f}{EIk^4[\alpha_f k \tanh(kH)/b + 1]} \tag{15}$$

Similar to Eq.(11), a linear system of beam kinematics Eq.(16) can be obtained by solving the ODE Eq.(14) analytically.

$$\begin{bmatrix} \hat{w}_n \\ \hat{v}_n \\ \hat{a}_n \end{bmatrix} = \mathbf{C_{RN}} \begin{bmatrix} \hat{w}_{n-1} \\ \hat{v}_{n-1} \\ \hat{a}_{n-1} \end{bmatrix} = \begin{bmatrix} (1-M_1)\cos(\omega_0 \Delta t) + M_1 & \frac{\sin(\omega_0 \Delta t)}{\omega_0} & M_2(1-\cos(\omega_0 \Delta t)) \\ -\omega_0(1-M_1)\sin(\omega_0 \Delta t) & \cos(\omega_0 \Delta t) & M_2 \omega_0 \sin(\omega_0 \Delta t) \\ -\omega_0^2(1-M_1)\cos(\omega_0 \Delta t) & -\omega_0 \sin(\omega_0 \Delta t) & M_2 \omega_0^2 \cos(\omega_0 \Delta t) \end{bmatrix} \begin{bmatrix} \hat{w}_{n-1} \\ \hat{v}_{n-1} \\ \hat{a}_{n-1} \end{bmatrix} \tag{16}$$

Hence, given an initial condition at t_0, the partitioned solution at certain t_n can be computed explicitly using Eq.(16). The stability criterion of R-N explicit coupling scheme is given by Eq.(17)

$$|\rho(\mathbf{C_{RN}})| \approx \Phi_{RN} = \left| \frac{1 - \alpha_f \rho_f / (\rho_s bh)}{\alpha_f k \tanh(kH)/b + 1} \right| \leq 1 \tag{17}$$

$|\rho(\mathbf{C_{RN}})| = \Phi_{RN}$ if Δt goes to zero. Eq.(17) indicates that, in addition to the physical parameters, the numerical stability of the Robin-Neumann scheme depends on the choice of α_f. By introducing three new non-dimensional parameters $\alpha = \alpha_f k/b$, $C_h = kh$, $C_H = kH$, we can rewrite Eq.(17).

$$\Phi_{RN}(\eta, C_h, C_H, \alpha) = \left| \frac{\eta - \alpha/C_h}{\eta + \alpha\eta \tanh(C_H)} \right| \leq 1 \tag{18}$$

Figure 3 shows the dependence of Φ_{RN} on density ratio and C_H for different values of non-dimensional combination parameter α. As can be seen from figure 3(a), for problems where the solid and fluid densities are similar, e.g., blood flow in arteries where $\eta \approx 1$, the R-N explicit coupling scheme is stable if a sufficiently

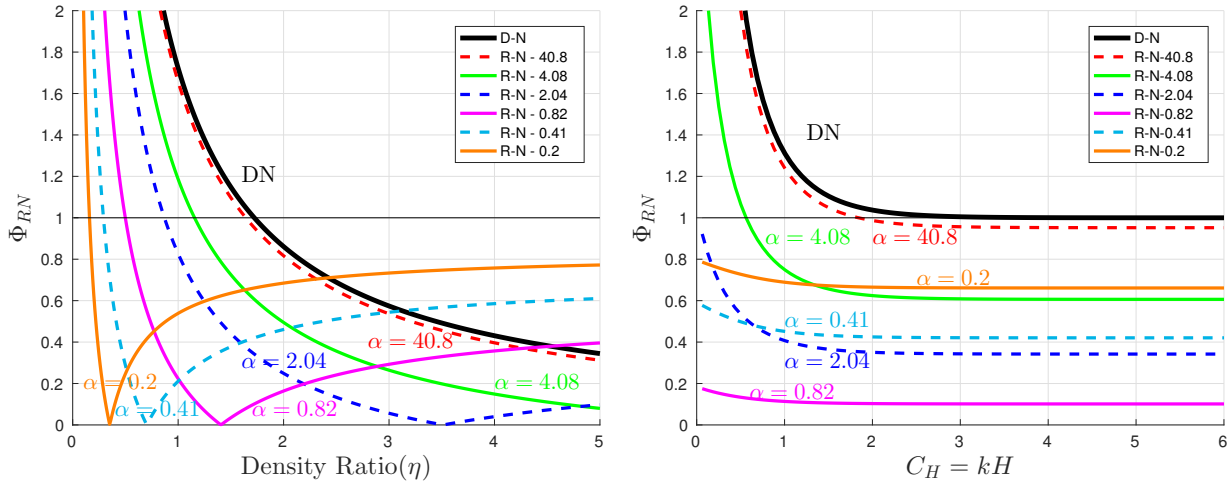

(a) (b)

Figure 3: (a) Dependence of Φ on density ratio η. (b) Dependence of Φ on non-dimensional parameter C_H.

small α is used. Similarly, from figure 3(b), α should be small enough for a given slender fluid domain in order to ensure the numerical stability of the R-N explicit coupling scheme. In other words, as α_f is reduced, the R-N explicit coupling scheme remains stable under a wider region of the physical parameter space. However, the combination parameter cannot be made arbitrarily small due to the lost of accuracy. This is because, as combination parameter is reduced, the influence of kinematic condition at fluid-structure interface is suppressed. Consider an extreme case where $\alpha_f = 0$; in this case, the Robin-Neumann scheme becomes equivalent to the Neumann-Neumann scheme and one of the transmission conditions for coupled system - the kinematic condition - is missing. Hence, characterizing the effect of combination parameter on accuracy is needed (to be discussed in section C).

C. Numerical Experiments

In this section, we present some results of the numerical solution of 2D model problem based on R-N explicit coupling scheme with the aim of verifying the mathematical analysis carried out in Section B. First, we verify the stability criterion for the Robin-Neumann scheme Eq.(17). Second, the numerical error and the order of accuracy of the R-N explicit coupling scheme using different values of the combination parameter α_f are shown to demonstrate the effect of α_f on accuracy. Referring to the domain of Fig.2, we set $H = 1$ m, $b = 0.01540$ m, $h = 0.0924$ m, $L = 1$ m for all of the numerical tests. The initial condition of beam's kinematic at $t_0 = 0$ is obtained from exact solution and given as Eq.(19). For other parameters, we take $k = 2\pi$, $E = 70$ GPa, $I_z = 1 \times 10^{-6}$ m^4, $\rho_s = 1000$ kg/m^3, $\rho_f = 876$ kg/m^3, $\tilde{w} = 0.01$ m. The quantity of interest we show in this section is beam displacement at $x = 0.25$.

$$W(x, t_0) = 0, \qquad \frac{\partial W_n}{\partial t}|_{t_0} = 2\tilde{w}\omega \sin(kx), \qquad \frac{\partial^2 W_n}{\partial t^2}|_{t_0} = 0 \tag{19}$$

where $\tilde{w}$ denotes the vibration amplitude, and the frequency of beam vibration is $\omega = \sqrt{\frac{EIk^4}{\rho_s bh + \rho_f b/[k \tanh(kH)]}}$.

1. *Verification of stability criterion:*

It can be seen from the stability criterion Eq.(17) that, for a given combination of physical parameters, there is a critical value of α_f such that $\Phi = 1$, which is denoted by $\alpha_{f,c}$.

$$\alpha_{f,c} = \frac{2\rho_s bh}{\rho_f - \rho_s hk \tanh(kH)} \tag{20}$$

Downloaded by VIRGINIA TECH on July 12, 2018 | http://arc.aiaa.org | DOI: 10.2514/6.2017-3447

Given the physical values above, it turns out to be $\alpha_{f,c} \simeq 0.0096328$. The R-N explicit coupling scheme with an α_f above this critical value is predicted to be unstable. Hence, the critical value $\alpha_{f,c}$ and a slightly higher value $1.05\alpha_{f,c}$ are tested in order to verify Eq.(17). The results of the partitioned solution with these two values of α_f are shown in figure 4(a) and figure 4(b). The solution is stable if α_f is set to be the critical value $\alpha_{f,c}$ as shown in figure 4(a). However, numerical instability is observed in figure 4(b) where $\alpha_f = 1.05\alpha_{f,c}$. It can thus be concluded that $\alpha_{f,c}$ is the critical value of combination parameter for numerical stability, which verifies the stability criterion Eq.(17). It is worth mentioning that compared to R-N scheme with $\alpha_f = 1.05\alpha_{f,c}$, the solution blows up even faster if the D-N scheme (which is a particular case of the R-N scheme where $\alpha_f = \infty$) is used.

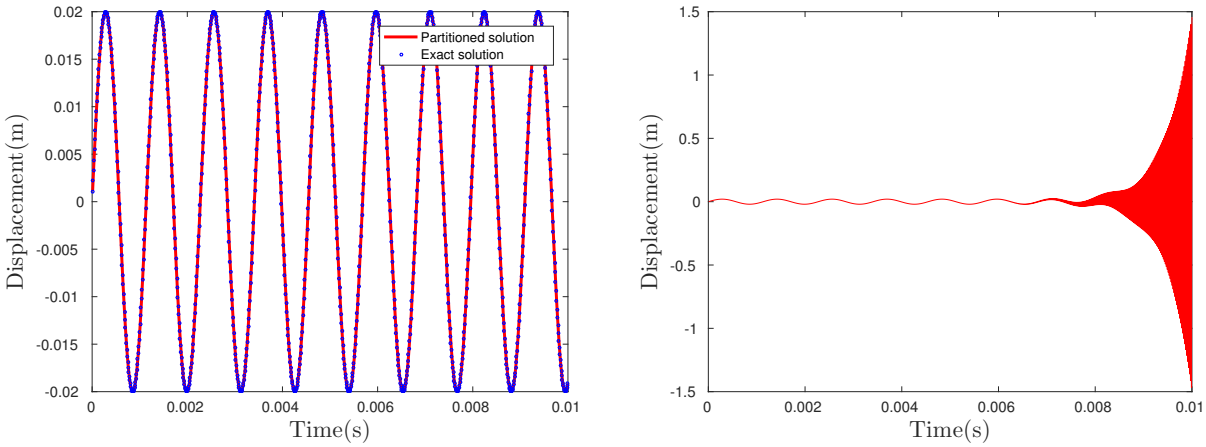

Figure 4: Partitioned solution of beam displacement at $x = 0.25$ using Robin-Neumann explicit coupling scheme with two different combination parameters: (a) $\alpha_f = \alpha_{f,c}$ and (b) $\alpha_f = 1.05\alpha_{f,c}$.

2. Effect of α_f on accuracy:

In this section, we characterize the effect of α_f on the accuracy of the R-N explicit coupling scheme by comparing the results of numerical tests using different α_f. The α_f should be chosen such that the numerical solution is stable. Hence, two special values of α_f that satisfy stability criterion Eq.(17) are considered here. One is the critical value $\alpha_{f,c}$ defined in Eq.(20) and the other one is an added-mass-free α_f, denoted by $\alpha_{f,amf}$, which is chosen such that $\Phi_{RN} = 0$. Given physical values above, two values turn out to be $\alpha_{f,c} \simeq 0.0096328$ and $\alpha_{f,amf} \simeq 0.0016244$. Figure 5(a) compares the time-history of error of beam displacement at $x = 0.25$ between two test cases. The error is computed using the exact solution of model problem. It can be clearly seen that the amplitude of error for the R-N scheme with $\alpha_{f,amf}$ is much higher than that with the critical value $\alpha_{f,c}$. Figure 5(b) shows that the R-N explicit coupling scheme with $\alpha_{f,c}$ is second-order accurate in time while it is first-order accurate if $\alpha_{f,amf}$ is used. These results indicate that the combination parameter in the Robin transmission condition affects the order of accuracy of a partitioned procedure and an optimal α_f in terms of accuracy can be chosen such that $\Phi = 1$.

$$\alpha_{f,opt} = \alpha_{f,c} = \frac{2\rho_s bh}{\rho_f - \rho_s hk \tanh(kH)} \tag{21}$$

This finding provides us with an idea to determine the optimal α_f for general FSI problems such that the Robin-Neumann scheme can achieve it best accuracy while also retaining numerical stability.

III. An Embedded Boundary CFD-CSD Framework with Robin-Neumann Interface Condition

In this section, we present a novel embedded boundary method that couples a projection-based incompressible flow solver with a finite element beam structure using the Robin-Neumann interface condition

Downloaded by VIRGINIA TECH on July 12, 2018 | http://arc.aiaa.org | DOI: 10.2514/6.2017-3447

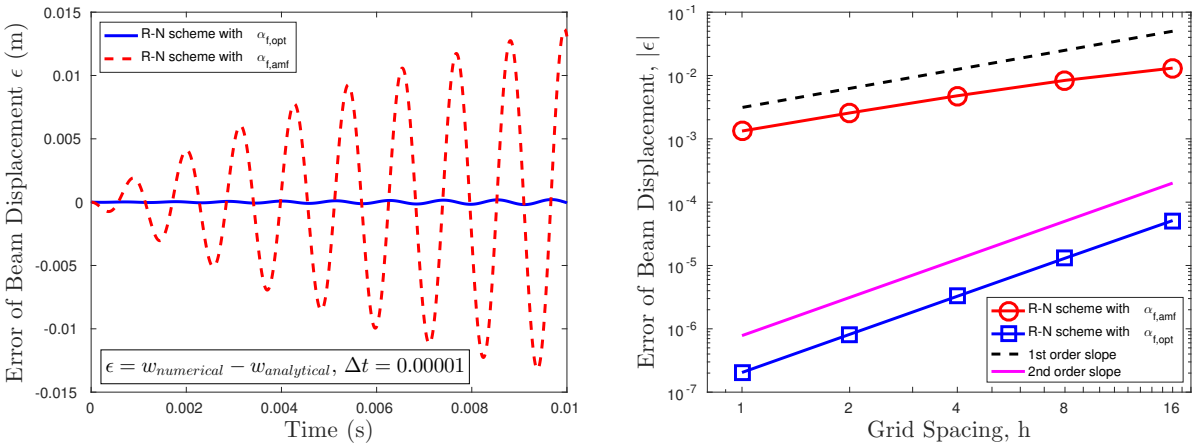

(a) (b)

Figure 5: (a) Comparison of error magnitude. (b) Comparison of the order of accuracy

Downloaded by VIRGINIA TECH on July 12, 2018 | http://arc.aiaa.org | DOI: 10.2514/6.2017-3447

discussed in Section II. Let $\Omega_f \subset \mathbb{R}^2$ denotes the domain of fluid, governed by incompressible Navier-Stokes (N-S) equations Eq.(22).

$$\begin{cases} \nabla \cdot \mathbf{U} = 0 & \text{(22a)} \\ \dfrac{\partial \mathbf{U}}{\partial t} + \mathbf{U} \cdot \nabla \mathbf{U} = \nu \Delta \mathbf{U} - \dfrac{1}{\rho_f} \nabla P & \text{(22b)} \end{cases}$$

where t denotes time, ρ_f the fluid density, $\mathbf{U} = (u, v)$ the fluid velocity, P the fluid pressure and ν the kinematic viscosity. Here, the fluid is assumed to be laminar. The structure governing equation defined in $\Omega_s \subset \mathbb{R}^2$ is written in Lagrangian formulation. Depending on the flexible structure of interest, different types of structure governing equations can be applied, e.g., equation of motion for nonlinear elastic structures[23] or equation of motion for linear elastic structures. For the sake of simplicity, we start with a linear elastic structure governed by Eq.(23).

$$\rho_s \frac{\partial^2 \mathbf{d}}{\partial t^2} - \nabla \cdot \sigma_s = \mathbf{f} \tag{23}$$

where, $\mathbf{d}$ denotes the displacement vector of the structure, ρ_s the structure density, σ_s the Cauchy stress tensor with $\sigma_s = -p\mathbf{I} + 2\mu\epsilon$, $\mathbf{f}$ the body force per unit volume. At fluid-structure interface $\Sigma = \partial\Omega_f \cap \partial\Omega_s$, if we assume an impermeable interface, the interaction between fluid and structure is driven by two transmission conditions, i.e., kinematic condition Eq.(24a) and dynamic condition Eq.(24b).

$$\mathbf{U}_j = \frac{\partial \mathbf{d}_j}{\partial t} \qquad \text{on } \Sigma \qquad j = 1, 2 \tag{24a}$$

$$\sigma_f \cdot \mathbf{n} = \sigma_s \cdot \mathbf{n} \qquad \text{on } \Sigma \tag{24b}$$

where $\mathbf{n}$ denotes the unit normal to Σ and σ_f is fluid stress tensor.

A. Robin-Neumann partitioned procedure and time-integrator

To solve the coupled system Eq.(22)-Eq.(24), we apply Robin-Neumann implicit coupling scheme in which the two subsystems, fluid subsystem with Robin transmission condition and structure subsystem with Neumann transmission condition, are solved in the fashion of fixed-point iteration.

For the temporal discretization of fluid equations Eq.(22), we consider the second-order Hybrid Approximate Projection Method proposed in Griffith *et al.*[24] This hybrid method features the use of two classes of projection methods for incompressible N-S equation in order to reduce pressure oscillations induced by Embedded Boundary Method.[25] Specifically, at each time-step, the fluid velocity is updated using Incremental-Pressure Projection Method[26] and the updated pressure is determined by the Pressure-Free Projection Method.[27] Furthermore, in projection step, an approximate projection operator is applied to avoid

the difficulty caused by pressure-velocity decoupling in collocated grid, i.e. the so-called "checkerboard" issue.[28]

The Robin transmission condition for fluid subsystem at fluid-structure interface can be constructed by the linear combination of kinematic and dynamic condition, and it is time-discretized as Eq.(25).

$$\alpha_f \frac{U^{n+1,k+1} - U^n}{\Delta t} + \sigma_f^{n+1,k+1} \cdot \mathbf{n} = \alpha_f \left(\frac{\partial^2 \mathbf{d}}{\partial t^2} \right)^{n+1,k} + \sigma_s^{n+1,k} \cdot \mathbf{n} \tag{25}$$

where α_f is the combination parameter, Δt the time-step size. The superscript n denotes the time step and k is the index of sub-iteration at this time-step. To enforce Robin transmission condition in fluid time-integration using hybrid projection method, two correponding interface conditions for intermediate velocity and projection step should be derived from Eq.(25). Here, we apply an operator splitting scheme introduced in Fernández *et al.*[20] where they decompose Eq.(25) into normal and tangential components. The normal component is enforced in the solution of intermediate velocity while the latter one is taken into account in solving pressure-Poisson equation.

B. Non body-fitted spatial discretization

Embedded Boundary Method (EBM) is particularly suitable for FSI problems involving complex geometry, large structural deformation, and topological change (e.g., fracture). Thus, one main objective of our work is to apply Robin-Neumann scheme to EBM framework.

In EBM framework, the fluid is solved on a fixed non body-fitted mesh and the boundary surface of the flexible structure is embedded in the fluid domain (see figure 6(a)). In our ERBM, the incompressible N-S equations are semi-discretized on a fixed Cartesian grid by a classical Finite Difference Method[24] with a cell-centered, collocated arrangement of fluid variables. On the other hand, the structure governing equation written in Lagrangian formulation is semi-discretized by the Finite Element Method. To impose the effect of embedded structure on the fluid, we consider the finite-difference based Ghost-Cell Method[29,30] in which the interface conditions at embedded boundary are enforced through the use of ghost-cells inside embedded structure (see figure 6(b)). A local reconstruction scheme is applied to determine the value of fluid variables at the ghost-cells. Take figure 6(b) as an example. The ghost-cell velocity $\mathbf{U}_G$ can be extrapolated from the given velocity interface condition $\mathbf{U}_B$ and the velocity at an imaginary point I which is computed by interpolating velocities at neighboring fluid cells $\mathbf{U}_1$-$\mathbf{U}_3$. This implicit incorporation of interface conditions introduces no forcing term in fluid governing equation and it retains a "shape" representation of embedded boundary.

As shown in figure 6(b), even though an irregular embedded boundary Σ is consider, the local reconstruction of ghost-cell for Dirichlet-type interface condition on Σ is straightforward. However, in projection step, we need to solve a pressure-Poisson equation subjected to Robin-type interface condition. The local reconstruction becomes challenging due to the discretization of normal derivative at the irregular boundary. Here, we employ a second-order accurate Shortley-Weller discretisation with a quadratic boundary treatment proposed in Jomaa *et al.*[31] to compute the value at ghost-cells for Robin-type interface condition.

C. Numerical experiment: The Turek & Hron benchmark problem

The fluid-structure coupled computational framework is validated using Turek & Hron benchmark problem.[32] The benchmark problem involves a two-dimensional laminar incompressible channel flow around a flexible beam which is mounted on the back of a fixed cylinder. The detailed geometry of this problem is shown in figure 7. In the fluid domain, no-slip boundary condition is enforced on top and bottom wall. The inflow boundary condition at the left channel is set to be a parabolic velocity profile:

$$u(0, y) = 1.5\bar{U} \frac{y(H - y)}{(H/2)^2}, \qquad v(0, y) = 0 \tag{26}$$

where H is the height of the fluid domain and $\bar{U}$ is the average inflow velocity. At the right channel outflow, a "*do nothing*" boundary condition is applied. The test case presented here is FSI2 in benchmark paper whose parameter settings are given in Table.1. As a test, the combination parameter used in Robin transmission condition Eq.(25) is set to be $\alpha_f = 10$.

Downloaded by VIRGINIA TECH on July 12, 2018 | http://arc.aiaa.org | DOI: 10.2514/6.2017-3447

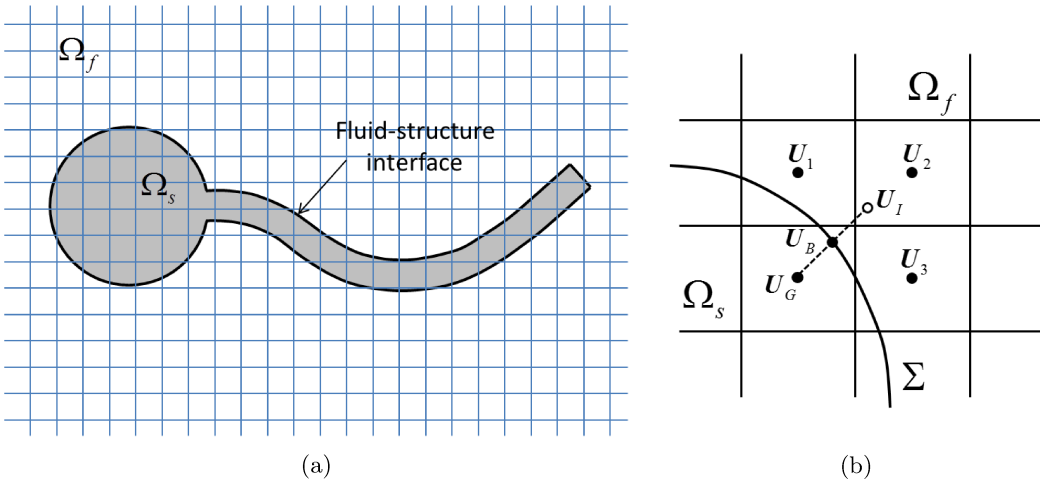

(a) (b)

Figure 6: (a) Schematic representation of the structure embedded in fluid domain. (b) An example illustration of local reconstruction of velocity for ghost-cell (G) using interface condition on embedded structure at B and velocities at neighboring fluid cells 1,2,3.

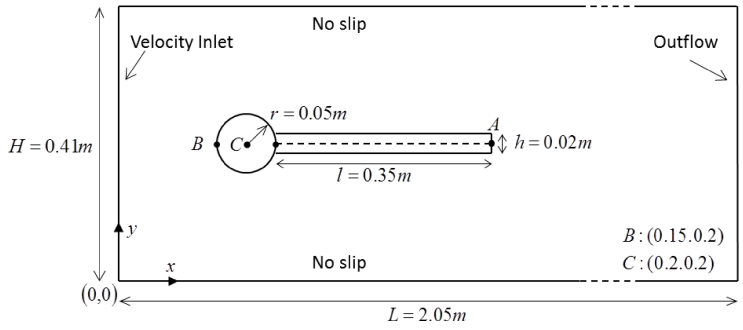

Figure 7: Geometry of the Turek & Hron FSI Benchmark

parameter	Value
$\rho_s[\frac{kg}{m^3}]$	1.0×10^4
ν_s	0.4
$\mu_s[\frac{kg}{ms^2}]$	5.0×10^5
$\rho_f[\frac{kg}{m^3}]$	1×10^3
$\nu_f[\frac{m^2}{s}]$	1×10^{-3}
$\bar{U}[\frac{m}{s}]$	1
Re	100

Table 1: Parameter settings for test case FSI2 (densities ρ_s,ρ_f, Poisson ratio ν_s, shear modulus μ_s, dynamics viscosity μ_f and kinematic viscosity ν_f)

Figure 8 shows the velocity magnitude of fluid and the beam deformation at four time instants in one period of beam vibration. Figure 9 shows the corresponding pressure field. It can be seen that when the flow past around the cylinder, it generates vortex shedding which induces vibration on the flexible beam. The plot for the tip (point A) displacement in y direction is shown in figure 10. The tip displacement varies between $\delta y \in [-0.1817, 0.1761]$.

Remark: It is notable that the predicted tip displacement shown in Figure 10 is not the same as the benchmark solution. This is because the flexible beam is modeled as a linear elastic beam in our current computational framework, despite the large deformation. A two-dimensional non-linear elastic beam model will be implemented in future work.

Downloaded by VIRGINIA TECH on July 12, 2018 | http://arc.aiaa.org | DOI: 10.2514/6.2017-3447

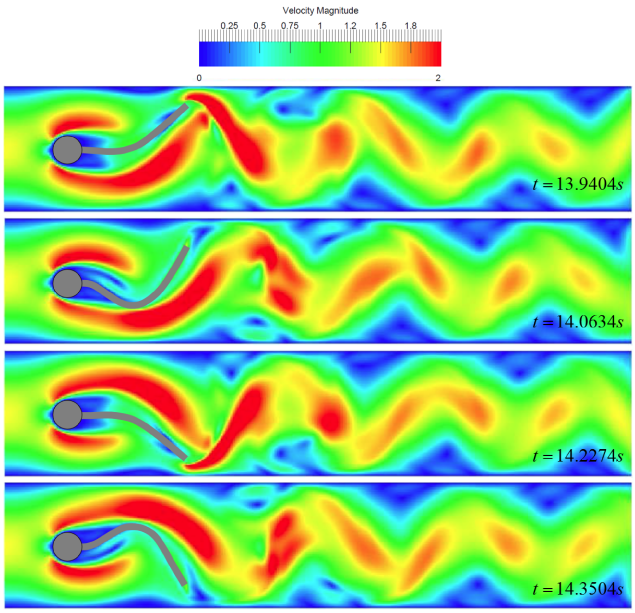

Figure 8: Snapshots of velocity magnitude inside one period of beam vibration

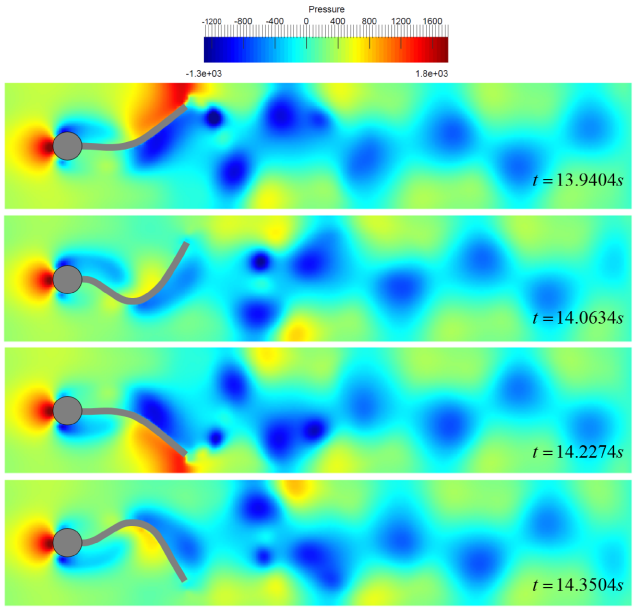

Figure 9: Snapshots of velocity magnitude inside one period of beam vibration

Downloaded by VIRGINIA TECH on July 12, 2018 | http://arc.aiaa.org | DOI: 10.2514/6.2017-3447

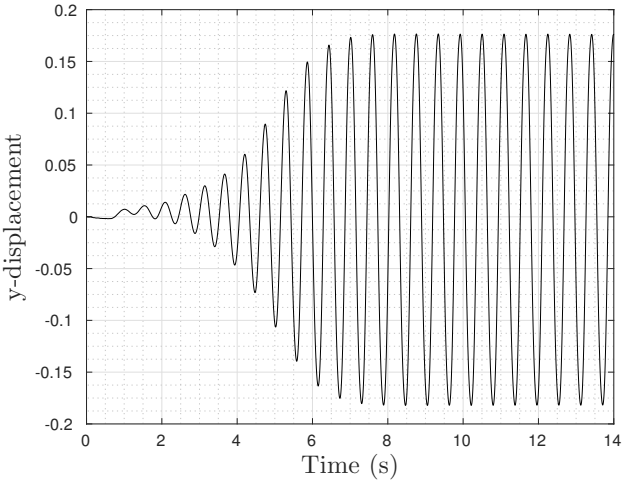

Figure 10: Tip displacement in y-direction

Downloaded by VIRGINIA TECH on July 12, 2018 | http://arc.aiaa.org | DOI: 10.2514/6.2017-3447

IV. Conclusions

This paper investigates the partitioned solution of fluid-structure interaction problems involving incompressible flow and large fluid-structure density ratio. This type of problems is often challenging for two reasons. First, partitioned solvers are subjected to numerical instability due to the amplification of error at fluid-structure interface (i.e. the artificial added-mass effect). Second, the structure may undergo large deformation, which translates to large deformation of the CFD domain. We present an embedded Robin boundary method that addresses both issues. Specifically, we replace the traditional Dirichlet-Neumann interface condition by a one-parameter (i.e. α_f) Robin-Neumann interface condition. The two conditions are mathematically equivalent. However, previous studies have shown that when α_f is carefully chosen, the latter may improve the stability property of partitioned solvers. Moreover, we also employ an embedded boundary method to discretize the fluid governing equations, which naturally accommodates arbitrary structural motion and deformation. While both the Robin-Neumann interface condition and embedded boundary methods have been proposed before, the combination of the two is a novelty of the present work. Furthermore, to rigorously investigate the effects of α_f on partitioned solvers, we consider a two-dimensional model problem and solve it using an analytical partitioned procedure, which does not involve spatial discretization nor numerical time-integration. The solution indicates that α_f affects both numerical stability and the order of accuracy. We have also identified a variable Φ, as a function of α_f, which can be used to derive an optimal value of α_f.

Acknowledgments

S.C. and K.W. acknowledge the support by the Institute for Critical Technologies and Applied Sciences (ICTAS) at Virginia Tech through a Junior Faculty Collaboration (JFC) project. K.W. also acknowledges the support by the Air Force Office of Scientific Research (AFOSR) through a summer faculty fellowship.

References

[1]Badia, S., Nobile, F., and Vergara, C., "Fluid–structure partitioned procedures based on Robin transmission conditions," *Journal of Computational Physics*, Vol. 227, No. 14, 2008, pp. 7027–7051.

[2]Hübner, B., Walhorn, E., and Dinkler, D., "A monolithic approach to fluid–structure interaction using space–time finite elements," *Computer methods in applied mechanics and engineering*, Vol. 193, No. 23, 2004, pp. 2087–2104.

[3]Michler, C., Hulshoff, S., Van Brummelen, E., and De Borst, R., "A monolithic approach to fluid–structure interaction," *Computers & fluids*, Vol. 33, No. 5, 2004, pp. 839–848.

[4]Felippa, C. A., Park, K., and Farhat, C., "Partitioned analysis of coupled mechanical systems," *Computer methods in applied mechanics and engineering*, Vol. 190, No. 24, 2001, pp. 3247–3270.

[5]Matthies, H. G. and Steindorf, J., "Partitioned strong coupling algorithms for fluid–structure interaction," *Computers &*

Structures, Vol. 81, No. 8, 2003, pp. 805–812.

[6]Causin, P., Gerbeau, J.-F., and Nobile, F., "Added-mass effect in the design of partitioned algorithms for fluid–structure problems," *Computer methods in applied mechanics and engineering*, Vol. 194, No. 42, 2005, pp. 4506–4527.

[7]Förster, C., Wall, W. A., and Ramm, E., "Artificial added mass instabilities in sequential staggered coupling of nonlinear structures and incompressible viscous flows," *Computer methods in applied mechanics and engineering*, Vol. 196, No. 7, 2007, pp. 1278–1293.

[8]Wang, K., Lea, P., and Farhat, C., "A computational framework for the simulation of high-speed multi-material fluid–structure interaction problems with dynamic fracture," *International Journal for Numerical Methods in Engineering*, Vol. 104, No. 7, 2015, pp. 585–623.

[9]Lakshminarayan, V., Farhat, C., and Main, A., "An embedded boundary framework for compressible turbulent flow and fluid–structure computations on structured and unstructured grids," *International Journal for Numerical Methods in Fluids*, Vol. 76, No. 6, 2014, pp. 366–395.

[10]Farhat, C., Wang, K., Main, A., Kyriakides, S., Lee, L.-H., Ravi-Chandar, K., and Belytschko, T., "Dynamic implosion of underwater cylindrical shells: experiments and computations," *International Journal of Solids and Structures*, Vol. 50, No. 19, 2013, pp. 2943–2961.

[11]Farhat, C. and Lakshminarayan, V. K., "An ALE formulation of embedded boundary methods for tracking boundary layers in turbulent fluid–structure interaction problems," *Journal of Computational Physics*, Vol. 263, 2014, pp. 53–70.

[12]Lea, P. D., Farhat, C., and Wang, K. G., "A Fluid-Structure Coupled Computational Framework for Fluid-Induced Failure and Fracture," *ASME 2015 34th International Conference on Ocean, Offshore and Arctic Engineering*, American Society of Mechanical Engineers, 2015, pp. V05BT04A014–V05BT04A014.

[13]Wang, K. G., Lea, P., Main, A., McGarity, O., and Farhat, C., "Predictive simulation of underwater implosion: Coupling multi-material compressible fluids with cracking structures," *ASME 2014 33rd International Conference on Ocean, Offshore and Arctic Engineering*, American Society of Mechanical Engineers, 2014, pp. V08AT06A028–V08AT06A028.

[14]Farhat, C., Van der Zee, K. G., and Geuzaine, P., "Provably second-order time-accurate loosely-coupled solution algorithms for transient nonlinear computational aeroelasticity," *Computer methods in applied mechanics and engineering*, Vol. 195, No. 17, 2006, pp. 1973–2001.

[15]Guidoboni, G., Glowinski, R., Cavallini, N., and Canic, S., "Stable loosely-coupled-type algorithm for fluid–structure interaction in blood flow," *Journal of Computational Physics*, Vol. 228, No. 18, 2009, pp. 6916–6937.

[16]Bukač, M., Čanić, S., Glowinski, R., Tambača, J., and Quaini, A., "Fluid–structure interaction in blood flow capturing non-zero longitudinal structure displacement," *Journal of Computational Physics*, Vol. 235, 2013, pp. 515–541.

[17]Canic, S., Muha, B., and Bukac, M., "Stability of the kinematically coupled\ beta-scheme for fluid-structure interaction problems in hemodynamics," *arXiv preprint arXiv:1205.6887*, 2012.

[18]Fernández, M. A., Gerbeau, J.-F., and Grandmont, C., "A projection algorithm for fluid–structure interaction problems with strong added-mass effect," *Comptes Rendus Mathematique*, Vol. 342, No. 4, 2006, pp. 279–284.

[19]Fernández, M. A., Mullaert, J., and Vidrascu, M., "Explicit Robin–Neumann schemes for the coupling of incompressible fluids with thin-walled structures," *Computer Methods in Applied Mechanics and Engineering*, Vol. 267, 2013, pp. 566–593.

[20]Fernández, M. A., Landajuela, M., and Vidrascu, M., "Fully decoupled time-marching schemes for incompressible fluid/thin-walled structure interaction," *Journal of Computational Physics*, Vol. 297, 2015, pp. 156–181.

[21]Li, L., Henshaw, W., Banks, J., Schwendeman, D., and Main, A., "A stable partitioned FSI algorithm for incompressible flow and deforming beams," *Journal of Computational Physics*, Vol. 312, 2016, pp. 272–306.

[22]Banks, J., Henshaw, W., and Schwendeman, D., "A stable partitioned FSI algorithm for incompressible flow and structural shells," *arXiv preprint arXiv:1308.5913*, 2013.

[23]Wang, K., Rallu, A., Gerbeau, J.-F., and Farhat, C., "Algorithms for interface treatment and load computation in embedded boundary methods for fluid and fluid–structure interaction problems," *International Journal for Numerical Methods in Fluids*, Vol. 67, No. 9, 2011, pp. 1175–1206.

[24]Griffith, B. E. and Peskin, C. S., "On the order of accuracy of the immersed boundary method: Higher order convergence rates for sufficiently smooth problems," *Journal of Computational Physics*, Vol. 208, No. 1, 2005, pp. 75–105.

[25]Lee, L. and LeVeque, R. J., "An immersed interface method for incompressible Navier–Stokes equations," *SIAM Journal on Scientific Computing*, Vol. 25, No. 3, 2003, pp. 832–856.

[26]Bell, J. B., Colella, P., and Glaz, H. M., "A second-order projection method for the incompressible Navier-Stokes equations," *Journal of Computational Physics*, Vol. 85, No. 2, 1989, pp. 257–283.

[27]Chorin, A. J., "Numerical solution of the Navier-Stokes equations," *Mathematics of computation*, Vol. 22, No. 104, 1968, pp. 745–762.

[28]Drikakis, D. and Rider, W., *High-resolution methods for incompressible and low-speed flows*, Springer Science & Business Media, 2006.

[29]Tseng, Y.-H. and Ferziger, J. H., "A ghost-cell immersed boundary method for flow in complex geometry," *Journal of computational physics*, Vol. 192, No. 2, 2003, pp. 593–623.

[30]Mittal, R., Dong, H., Bozkurttas, M., Najjar, F., Vargas, A., and von Loebbecke, A., "A versatile sharp interface immersed boundary method for incompressible flows with complex boundaries," *Journal of computational physics*, Vol. 227, No. 10, 2008, pp. 4825–4852.

[31]Jomaa, Z. and Macaskill, C., "Numerical solution of the 2D Poisson equation on an irregular domain with Robin boundary conditions," *ANZIAM Journal*, Vol. 50, 2008, pp. 413–428.

[32]Turek, S. and Hron, J., "Proposal for numerical benchmarking of fluid-structure interaction between an elastic object and laminar incompressible flow," *Fluid-structure interaction*, Springer, 2006, pp. 371–385.

Downloaded by VIRGINIA TECH on July 12, 2018 | http://arc.aiaa.org | DOI: 10.2514/6.2017-3447